Sol-gel route synthesis of high energy density Li [Li 0. 2 Ni 0 . 3 Mn0 .7] O 2 cathode with controlled structure, morphology and enhanced electrochemical performance

Article *in* Energy Storage · November 2022

DOI: 10.1002/est2.427

CITATIONS
0

READS
99

5 authors, including:

Prettencia L Joseph
Vels University
6 PUBLICATIONS **6** CITATIONS
SEE PROFILE

Roselin Ranjitha Mathiarasu
11 PUBLICATIONS **132** CITATIONS
SEE PROFILE

Raghu Sangeetha
Oregon State University
71 PUBLICATIONS **2,057** CITATIONS
SEE PROFILE

Received: 30 September 2022 | Revised: 14 November 2022 | Accepted: 17 November 2022

DOI: 10.1002/est2.427

RESEARCH ARTICLE

ENERGY STORAGE WILEY

Sol-gel route synthesis of high energy density Li $[Li_{0.2}Ni_{0.3}Mn0_{.7}]$ O_2 cathode with controlled structure, morphology and enhanced electrochemical performance

Leonard Joseph Prettencia[1] | **Elumalai Soundarrajan**[1] | **Mathiarasu Roselin Ranjitha**[2] | **Raman Kalaivani**[1] | **Subashchandrabose Raghu**[3]

[1]Department of Chemistry, Vels Institute of Science, Technology & Advanced Studies (VISTAS), Chennai, Tamilnadu, India

[2]Department of Chemistry, Stella Maris College (Autonomous) Affiliated to University of Madras, Chennai, Tamilnadu, India

[3]Centre for Advanced Research and Development - Chemistry, Vels Institute of Science, Technology & Advanced Studies (VISTAS), Chennai, Tamilnadu, India

Correspondence
Raman Kalaivani, Department of Chemistry, Vels Institute of Science, Technology & Advanced Studies (VISTAS), Chennai, Tamilnadu, India.
Email: rakvani@yahoo.co.in

Subashchandrabose Raghu, Centre for Advanced Research and Development - Chemistry, Vels Institute of Science, Technology & Advanced Studies (VISTAS), Chennai, Tamilnadu, India.
Email: subraghu_0612@yahoo.co.in

Abstract

The desire for long driving range and low cost of electric vehicles necessitates the use of superior rechargeable lithium batteries. These batteries with enhanced energy density addresses the demand for cutting-edge cathode materials which can deliver amplified voltage and capacity. Lithium-rich manganese is one among such promising cathodes for lithium-ion batteries. In this work, three different organic acids, including oxalic (OX), tartaric (TA) and ascorbic (AS) acids were used to synthesis Li $[Li_{0.2}Ni_{0.3}Mn_{0.7}]$ O_2 (LNMO) materials with three unique microstructures. Physicochemical and electrochemical characterization techniques were used to investigate a range of properties. Electrochemical investigations demonstrated regulated morphology-enhanced electronic conductivity, increased energy density and prolonged cycle behavior. Among the three samples, AS-LNMO unveiled a capacity of 308.02 $mhAg^{-1}$ nearing the value of theoretical capacity. Whereas, TA-LNMO exhibited a remarkable stability even after 200 cycles with capacity retention of 99.3%. With specific discharge capacities of 308.02, 278, 252, 228 and 212 $mAhg^{-1}$ at 0.1C, 0.2C, 0.5C, 1C and 2C respectively, AS-LNMO exhibited superior rate capability. Collectively, this research offers valuable insights in using complexing agents which positively impacts the morphology and electrochemical performance of LNMOs in upcoming lithium-ion batteries.

KEYWORDS

complexing agents, good capacity retention, high energy density, sol-gel synthesis

1 | INTRODUCTION

Lithium-ion batteries and layered transition metal oxides remain in the spotlight due to their unique electrochemical performance. For decades, cathode materials containing layered $LiCO_2$, $LiMnO_2$, $LiFePO_4$, and $LiNi_xM_yCo_2O_2$ have dominated the LIB industry. These materials have energy densities of 600 $Whkg^{-1}$, which is not suitable in large-scale applications for electric vehicles and energy storage. As a result, the next-generation cathode materials face a criterion to have higher energy densities than any other materials. Fortunately, Li and Mn-rich layered oxide (LMRO) falls into this category of attaining high energy density and high theoretical capacity (280 $mAhg^{-1}$). In practical applications, its capacity exceeds even the theoretical value in the range of 280 to

350 $mAhg^{-1}$, depending on the proportion of Li-ions participating in the intercalation/de-intercalation process. The material's energy density increases roughly by 1000 $Whkg^{-1}$. Additionally, LMROs have a large operating voltage range as cathode materials ranging from 2 to 4.9 V. Due to such a wide operating voltage range, it serves as a suitable cathode material for the upcoming LIB production.[1,2]

As years progress, new protocols for the synthesis of hierarchical nano/micro structured materials with improved electrochemical performance are being developed and optimized. Several well-known methods that focus on influencing morphology in order to improve electrochemical performance include hydrothermal synthesis, carbonate co-precipitation, hydroxide process, solution combustion methods, solid state reactions and sol-gel process.[3-7]

Hydrothermal synthesis employed for LMRO cathode materials primarily resulted in octahedral-like particles with good crystallinity. In addition, the inclusion of suitable metal dopants were able to eliminate the impurity phases. Facile hydrothermal method suggested by Zhang et al. achieved a highest initial discharge capacity (352.8 $mAhg^{-1}$) with layered material and faded drastically after 50 cycles with a capacity retention of 75.5%.[8-11]

Co-precipitated LMRO materials exhibit well-matched layered behavior and a high initial discharge capacity. Most of the as-prepared samples display spherical and extremely porous micro-structure, high tap density, and agglomeration driven by diverse primary particle packing behavior. The surfactant or chelating agent used in the process regulates the morphology.[6,12,13] To produce polycrystalline materials from solid reagents, solid-state reactions are used as a typical synthesis technique where very high temperatures are used to induce the reaction. Chemical and morphological characteristics of the reagents such as surface area, reactivity, and free energy changes during the solid-state reaction, as well as other reaction parameters including pressure, temperature, and the reaction environment also influence the solid-state reaction. Large-scale manufacturing and simplicity are two benefits of such solid-state reaction approach.[14-16]

Whereas, sol–gel method is a simple, inexpensive, flexible, implementable, and effective chemical pathway for the synthesis of complex multicomponent compounds with a wide range of morphologies. Many factors including solvents, complexing agents, pH of solutions, and other parameters influencing the structure of materials also affect the electrochemical performance of the LMRO generated by sol-gel technique. The use of complexing agents has become a significant choice where the complexation between various complexing agents and transition metal ions is exposed visibly.

Few researchers have reported on sol-gel synthesis routes for LMRO cathode synthesis using complexing agents. Mehemet et al. prepared $Li_{1.2}Mn_{0.6}Ni_{0.35}Co_{0.15}O_2$ by self-ignition combustion process using glycine as complexing agent at discharge capacities 200, 250, and 290 $mAhg^{-1}$ at C, C/2, and C/4 rate. However, long-term cycling causes the ability to decline in capacity.[17] Pengdong et al. published a comparative study of Nickel Aluminium Cobalt (NCA) cathode materials synthesized by sol-gel technique with glycine, citric acid, and EDTA complexing agents. NCA-EDTA exhibited good electrochemical performance with an initial discharge of 175.1 $mAhg^{-1}$ at 0.2C and capacity retention of up to 97.3%.[18] According to Rong Yong et al., $LiFePO_4$/C prepared using the sol-gel method with acetic acid has a discharge capacity of 161.1 $mAhg^{-1}$ that decreased to 157.5 $mAhg^{-1}$ after 30 cycles.[19] Chenhao Zhao et al. reported a solid-state synthesis of $Li_{12}Ni_{0.16}Mn_{0.56}Co_{0.08}O_2$ using tartaric acid, citric acid, and oxalic acid complexing agents. At 0.1C, LNMC-Oxalic acid had the highest initial discharge of 267.52 $mAhg^{-1}$.[20] In this study, three different organic acids were used as complexing agents in the sol-gel method to prepare Li $[Li_{0.2}Ni_{0.3}Mn_{0.7}]$ O_2 composites.

The structure, morphology, and electrochemical performance of these Li-rich materials were thoroughly examined and compared with respect to the three complexing agents. A comparison and understanding of the benefits and drawbacks of effectively engaging different complexing agents are expected to aid in the selection of an appropriate organic acid for constructing a highly stable LMRO cathode structure with enhanced electrochemical performance.

2 | EXPERIMENTAL SECTION

2.1 | Preparation of LNMO-OX/TA/AS

The process of synthesizing $Li[Li_{0.2}Ni_{0.3}Mn_{0.7}]$ O_2 powders includes sol-gel formation, drying, pre-heat treatment, and high temperature sintering. The LMRO cathode material of given weight ratio $Li[Li_{0.2}Ni_{0.3}Mn_{0.7}]$ O_2 is prepared by sol-gel method with oxalic acid, tartaric acid, and ascorbic acid as complexing agents. The resultant products were labeled as LNMO-OX, LNMO-TA, and LNMO-AS. The metal precursors Mn $(NO_3)_2.6H_2O$ (Sigma Aldrich >99%) and $Ni(NO_3)_2.6H_2O$ (Sigma Aldrich >99%) were taken separately in 15 mL ethanol and sonicated for 20 min at room temperature. 1 M of each of the complexing agents (OX/TA/AS) were dissolved in 120 mL of deionized water accompanied with mild stirring at 480 rpm to generate a transparent solution that was kept at 120°C. Then, stoichiometric amount

of Li_2CO_3 was slowly added to the complexing agent solution. Further, the metal precursor solutions were fed into a burette and slowly dropped into the saturated complexing agent solution at 1 mL per minute rate. A greenish precipitate started to appear in all the three solutions with different complexing agents and the colour variation signified the reaction between the metal-complexing agents. Then the reaction mixture was adjusted to a pH of 10 to 11. The pH value of the metal precursor solution was tuned via predetermined amounts of ammonium hydroxide. Additionally, 5 mL of Polyethylene glycol was added as a surfactant. The reaction mixture was maintained at 120°C under stirring until a translucent sol was formed which then subsequently turned into a gel. The half-dried gel was burnt at 380°C for 3 h. Finally, the dried product was ground and fed into a tubular furnace for calcination at 430°C for 7 h at the rate of 4°C/min followed by sintering at high temperature 820°C for 10 h. The obtained products were slowly cooled to room temperature. Notably, all the heat treatments were done in air atmosphere.

2.2 | Material characterization

Phase determination and structure property relationship were explored and analysed by a Bruker D8 advance diffractometer using Cu-K_α radiation. The X-ray diffraction patterns were collected at room temperature in 2θ range 10° to 80°. The morphology and particle size of the sample were scrutinized on a high-resolution scanning electron microscope equipped with an energy dispersive X-ray spectrometer (EDX). HRTEM images were obtained using an electronic microscope JEOL model JEM-2010 (Pleasanton, CA, USA).[21]

2.3 | Electrochemical test

For analysing the electrochemical behavior of LMRO cathode, lithium anode-comprising cells were built. To fabricate the testing electrodes a slurry was created by mixing 80% active material, 15% acetylene black and 5% polyvinylidene fluoride binder in N-methyl-2-pyrrolidone solvent. In a vacuum oven at 80°C, the slurry was coated onto Al-foil and dried. Celgard 2400 microporous membrane was used as the separator (Celgard, LLC, Charlotte, NC, USA). The electrolyte was a 1 M $LiPF_6$ solution in a 1:1 combination of ethylene carbonate and dimethyl carbonate, and the anode was lithium foil. In electrochemical measurements, CR2032 coin cells were employed. The resulting sludge was evenly deposited onto a thin aluminium sheet with a thickness of 150 mm using an automated coating machine and vacuum-dried for 12 h at 120°C. The electrode materials were made into pellets with 10 mm diameter, active mass of 3 to 5 mg and were pressed for 5 s under 5 MPa. Finally, the half cells were placed together with pure lithium metal anode and 1 M $LiPF_6$ dissolved in EC/DMC/DEC (1:1:1) as an electrolyte. The cathode-to-anode active mass ratio was maintained at 1.7:1. In an argon-filled glove box (ETELUX Lab 2000) with water and oxygen concentrations of less than 1 ppm the cells were built in a systematic manner. Impedance measurements were carried out on a Biologic SP300 electrochemical work station utilizing a 5-mV amplitude AC sine wave in the range 100 kHz to 10 mHz to assess and compare the impedance responses. Before completing any EIS experiments the voltage responses of the cells were stabilized by resting them for several hours. The same setup was used for cyclic voltammetry (CV) studies in room temperature at 100 mVs^{-1} sweep rate. With a 0.01 mVs^{-1} CV scan rate the voltage range was observed to be 2.0 to 4.8 V. Then in a 2.0 to 4.8 V potential window, constant current discharge-charge and galvanostatic cycling studies were done at various rates adopting Neware battery testing equipment. (vs Li^+/Li).[22]

3 | RESULT AND DISCUSSION

3.1 | Structure, morphology, and composition analysis

3.1.1 | Metal complex mechanism

Scheme 1 represents the reaction between complexing agents and metal ions. The final product Li $[Li_{0.2}Ni_{0.3}Mn_{0.7}]$ O_2 showed that all three solutions OX-LNMO (mint green), TA-LNMO (lime green), and AS-LNMO (dark brownish) were formed with different colors. This variation in colors is due to the structure development that takes place at the molecular level of the diverse complexing agents with metal ions (M = Ni, Mn, Li).

Plausible mechanism of the metal-complex reaction is as follows:

(M = Mn, Ni) $NO_3.4H_2O + Li_2CO_3.H_2O$ + R-COOH → R-COO (M Li) + H_2O + HNO_3.

R-COO (MLi) + H_2O + HNO_3 → $Li_{1.2}Ni_{0.3}Mn_{0.7}O_2$ + H_2O + CO_2.

The lithium-rich layered oxides Li $[Li_{0.2}Ni_{0.3}Mn_{0.7}]$ O_2 were prepared by an organic assisted sol-gel process. In this process, the metal nitrates $M(NO_3).4H_2O$ were reacted with Li_2CO_3 in the presence of organic acids (oxalic, ascorbic & tartaric). On prolonged heating, the metal nitrates decomposed into metal nitrate hydroxides followed by which the dissociation of coordinated water

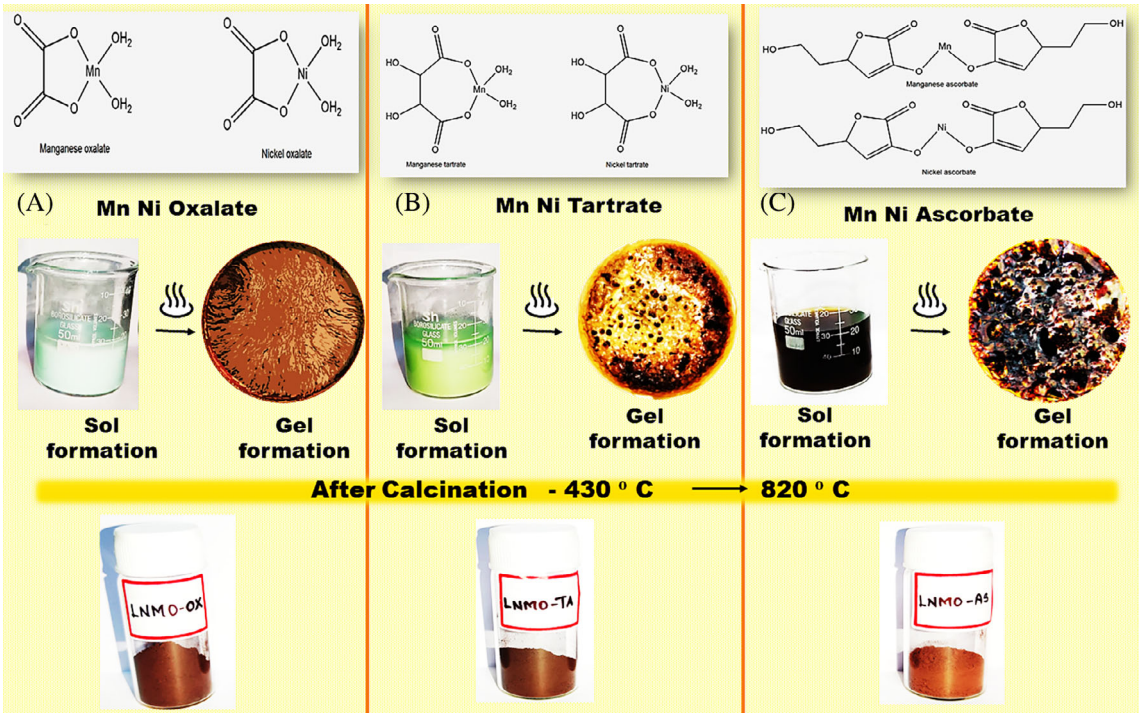

SCHEME 1 Representation of reaction between three different complexing agents and metal oxides

and oxygen happened. As a result of continual heat treatment, the sol that was generated in the process changed into the gel with varied hues and textures. The development of the metal complex R-COO (MLi) was caused by thermal behavior whereas the creation of an organometallic framework was caused by the cross-linking of metal complexes. When the temperature was raised the nitrate and organic molecules evacuated the metal-complex. NO_2 gas created during this process is not combustible, yet it is a strong oxidant that can effectively enhance the combustion energy and heat released. In addition, the heat emission can be ascribed to the combustion reaction of carbon and oxygen with accelerant NO_2 gas under moist conditions. Further on high-temperature calcination (430°C and then 820°C) the products attained dark brown colour characteristics of standard LMRO cathode materials. Although AS-LNMO sample showed a slightly different shade resembling red-soil.[20]

3.1.2 | *X-ray powder diffraction* analysis

The XRD patterns of Li $[Li_{0.2}Ni_{0.3}Mn_{0.7}]$ O_2 produced by sol-gel technique and calcined at 820°C are shown in Figure 1. The hexagonal α-$NaFeO_2$ structure was found in all the metal oxide samples complexed with three different organic acids. High refined peaks were observed at (003) and (104) are attributed to $LiMO_2$ phase (R3m). When compared to LNMO-OX, the strength of the fundamental peaks and additional peaks was sharper in LNMO-AS and LNMO-TA. All the samples had distinct peak splits at (006)/(102) and (108)/(110) which confirmed the material's layer properties in accordance with the previously reported data.

The weak peak at 20.7° of Li_2MnO_3 (C2/m space group) further implied that the Li_2MnO_3 phase (electrochemically inactive) was not entirely boosted by $LiMO_2$ phase to generate $LiMnO_2$ (electrochemically active). Therefore, Li_2MnO_3 co-existed partly with $LiMO_2$ and proved that the material could possibly be a composite. In addition, weak peaks of two more distinct phases were also detected. All the three samples had substantial Li_x-$Ni_{1-x}O_2$ (Cubic, Fm-3 m) and weak traces of spinel $LiMn_2O_4$ (Cubic, Fd-3 m) only in LNMO-OX.[23] Table 1. lists lattice parameters *a*, *c*, *c*/*a*, and I(003)/I(104), of the three samples. The lattice parameters do not differ significantly from one another when compared. The intensity ratio (R) of I(003)/I(104) depends on the distribution of cations in the crystal lattice and the extent of cation mixing of the substance. As R value rises, cation mixing becomes less intense. According to reports, when R is less than 1.2, unwanted cation mixing has been seen. When originally compared to AS-LNMO and TA-LNMO, the intensity ratio for OX-LNMO is greater than 1.2. The odred hexagonal structure of OX-LNMO may be one of the factors stabilizing the material's capacity up to 100 cycles. The intensity ratio after 100 cycles has been calculated, and it actually shows that while charging/

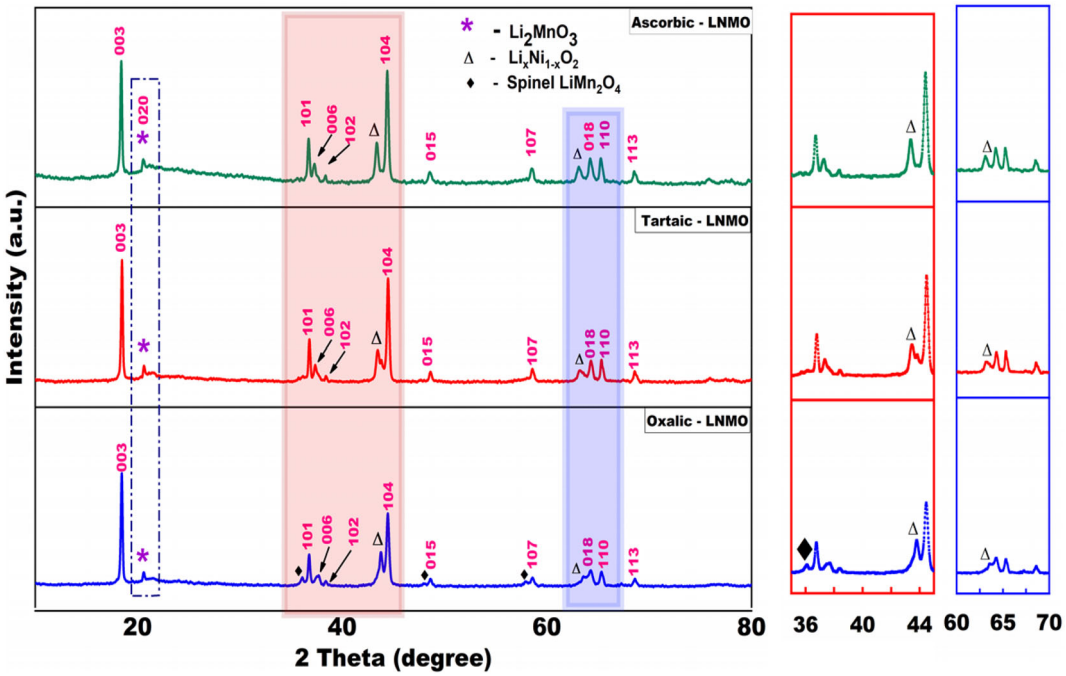

FIGURE 1 Representation of XRD patterns of Li $[Li_{0.2}Ni_{0.3}Mn_{0.7}]O_2$ prepared using different complexing agents

TABLE 1 Lists lattice parameters I(003)/I(104), c/a, a, and c of the three samples

Element	$a = b$	c	c/a	I(003)/I(104) Before 100 cycles	(003)/I(104) After 100 cycles
AS-LNMO	2.87	14.32	4.98	1.07	1.66
TA-LNMO	2.87	14.22	4.92	1.16	1.65
OX-LNMO	2.84	14.03	4.92	1.3	1.32

discharging the AS-LNMO and TA-LNMO samples' material stability was raised and their cation mixing was reduced by elevating the R value significantly, there was virtually no effect in the OX-LNMO sample.

Instead, in OX-LNMO peak intensity becomes very less intense than originally. Additionally, AS-LNMO and TA-LNMO appear to have a much-reduced amount of the $Li_xNi_{1-x}O_2$ (Cubic, Fm-3 m) electrochemically inactive phase in the following cycling. Figure S1, S2, and S3 represents the before and after 100 cycles XRD pattern of all the three samples. AS-LNMO and TA-LNMO samples are strongly restructured in the process charging/discharging, which actually leads the materials to have enhanced electrochemical behavior.

3.1.3 | Phase transition mechanism

According to Yi Pei et al., spinel phase dominates low temperature treated samples (ie, >700°C), and as the temperature rises the spinel phase concentration decreases correspondingly. Li is volatilized at higher temperatures (800°C-900°C) and increases the concentration of spinel which is formed at 850°C. As the temperature increases, more Li is intercalated into the guest frame work and the layered structures grow simultaneously. According to former studies when there is excessive Li content in the spinel phase (Li_2MnO_4), Li-rich spinel phase $Li_{1-x}Mn_{2-x}O_4$ would transform into Li_2MnO_3 and $Li_{1-x}Mn_{2-x}O_4$ at the transition temperature. Based on the literature review, the temperature has been optimized in this study and the samples were calcined at 820°C. Surprisingly, there were no obvious spinel phases in AS-LNMO and TA-LNMO (Figure 1) and the Li content is only moderately volatilized. Metal oxides complexed with oxalic acid (OX-LNMO) displayed more spinel phase when compared to AS-LNMO and TA-LNMO indicating that more Li content escaped from OX-weak LNMO's structural framework.[23-26]

3.1.4 | Raman spectroscopic analysis

The Raman shift spectra for all three samples are shown in Figure 2. All three profiles display two prominent bands at 490 cm^{-1} and 600 cm^{-1}, which correspond to

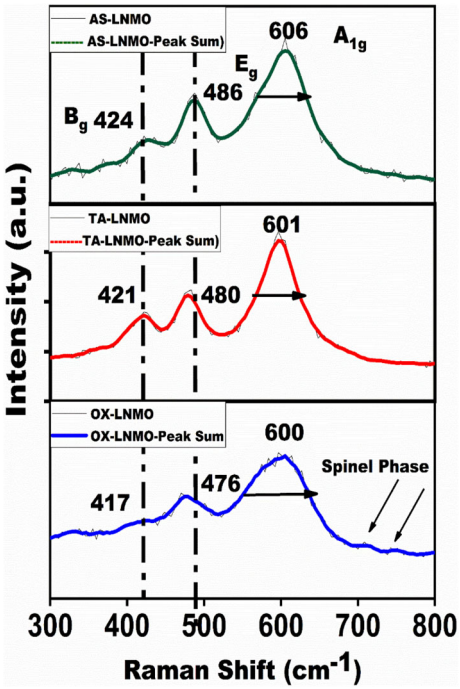

FIGURE 2 Representation of Raman Spectra of Li $[Li_{0.2}Ni_{0.3}Mn_{0.7}]O_2$ complexed with three organic acids

the Eg in plane O-M-O band and the A1g out of plane M-O stretch of the R3m space group, respectively ($LiMO_2$). In the instance of the OX-LNMO, it was noted that the primary bands at 476 cm^{-1} and 600 cm^{-1} appear to be diluted and lack a distinct peak.

For all three samples, the weak band at 427 cm^{-1} coincides with the Bg and Ag vibration of Li_2MnO_3. For AS-LNMO and TA-LNMO, the strong appearance of the weak band at 427 cm^{-1} demonstrates that Li_2MnO_3 is not fully activated and that, during the charging and discharging process, it can be electrochemically enhanced by $LiMO_2$, boosting the material's capacity. However, in the case of OX-LNMO, Li_2MnO_3 was already expired and nothing can be activated more, causing severe capacity fade and low-capacity value.

Only in OX-LNMO were smaller humps approximately 690 cm^{-1} to 700 cm^{-1} seen, indicating the presence of the spinel phase (shorter Mn-O).

3.1.5 | Scanning electron microscopy analysis and particle size

Figure 3 reveals the image of Li $[Li_{0.2}Ni_{0.3}Mn_{0.7}]O_2$ cathode materials prepared by sol-gel method with varied complexing agents. The SEM image unveils that all the three samples were crystalline in nature.

Figure 3A-C illustrates the morphology of AS-LNMO under three different magnifications. The AS-LNMO sample morphology resembled sea sponge-like irregular pores and voids. The secondary particles made up of small primary particles seemed to be polyhedral with definite edges. The morphology of TA-LNMO is depicted in Figure 3D-F which resembled an abnormal packed arrangement of porous coral reef-like structures. The pores were interlinked cellular structures with well-defined porosity and organized pores that were aligned in a periodic pattern.

The primary particles were in nanometre range and were aggregated together. Figure 3G-I represents the morphology of OX-LNMO which typically looked like sea algae's surface with mild porous nature. The primary particles were agglomerated and slightly bigger.

Figure 4 depicts the particle size distribution of Li $[Li_{0.2}Ni_{0.3}Mn_{0.7}]O_2$ cathode materials prepared by sol-gel method with complexing agents. The average particle size of AS-LNMO was comparatively smaller than the other two samples. The metal ions complexed with different organic acids (ascorbic, tartaric, and oxalic) followed the pattern: OX-LNMO > TA-LNMO > AS-LNMO. The primary particles were in nanometre range and the aggregated coarser particles influenced the materials electrochemical properties. Material with smaller particle size had the higher surface area and thereby facilitated for higher specific capacity. On the other hand, a higher surface area can also provide ample active sites for unnecessary side reactions such as the formation of an SEI layer. Reduced particle size allowed for shorter ion diffusion distances, whereas the large open-frame structures of AS-LNMO promoted rapid ionic diffusion.

The small particle size was responsible for the improved cycle life since, the smaller the particle the lower the stress and so the particle pulverization was reduced. Reduced particle size also improved the rate capacity, however with a broad particle distribution of OX-LNMO the rate capability was dominated by coarser particles.[27-29]

3.1.6 | High resolution - transmission electron microscopy

Figure 5A,B shows the smallest particle size (50-100 nm) of the sample prepared with ascorbic and tartaric acid. Figure 5C shows the fine nano sheets of oxalic acid and the size of OX-LNMO to be 200 nm-1 μm. In addition, the samples AS-LNMO and TA-LNMO had a definite edge with distinctive forms. AS-LNMO was more geometrically similar to a pentagonal dodecahedron with 12 pentagonal (faces) surfaces, 30 edges, and 20 corners. Whereas, TA-LNMO was more similar to a hexagonal prism with 8 (faces) surfaces, 18 edges, and 12 corners.

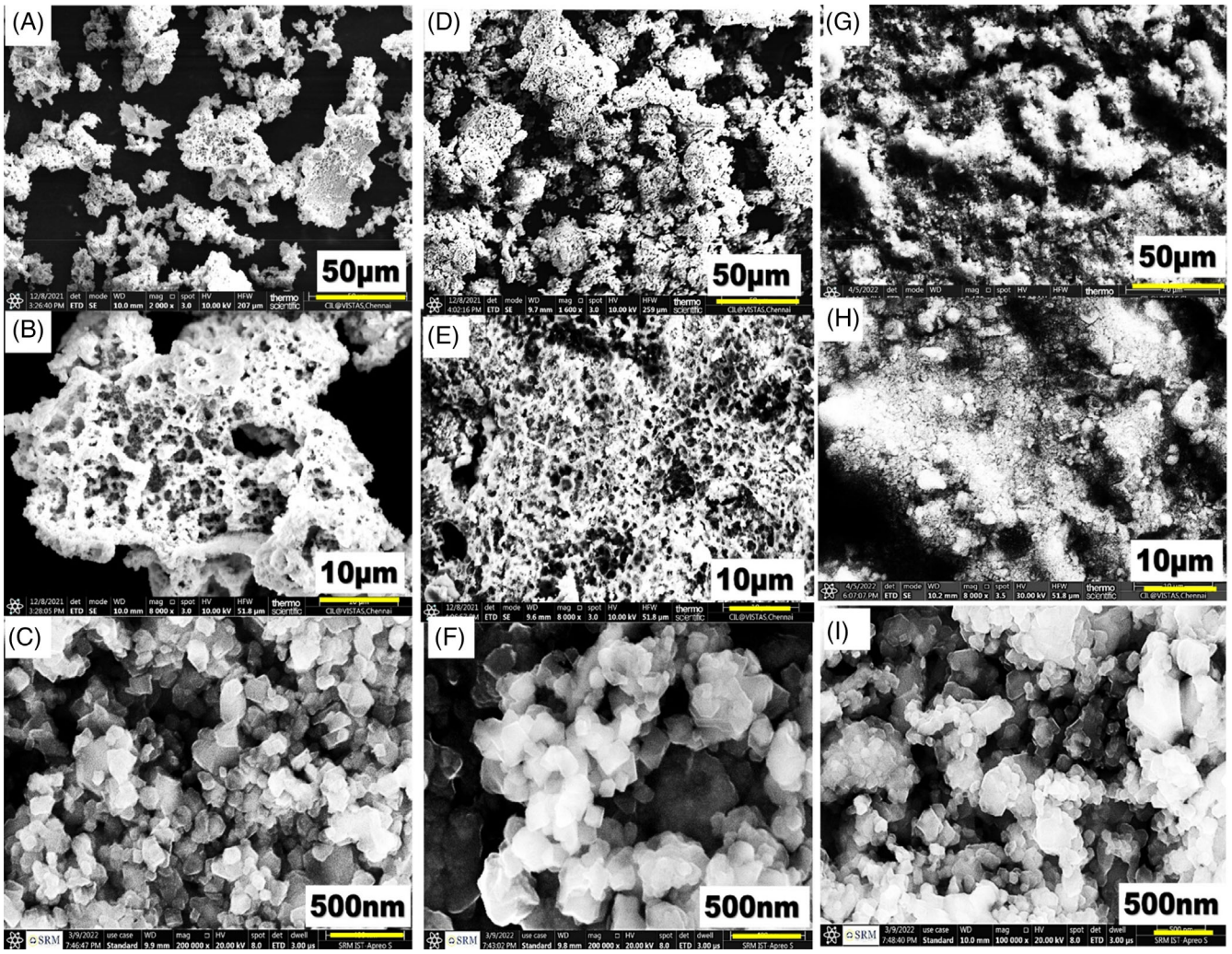

FIGURE 3 Representation of FE-SEM images of Li $[Li_{0.2}Ni_{0.3}Mn_{0.7}]O_2$ under three magnifications with different complexing agents. (A-C) AS-LNMO, (D-F) TA - LNMO, (G-I) OX-LNMO

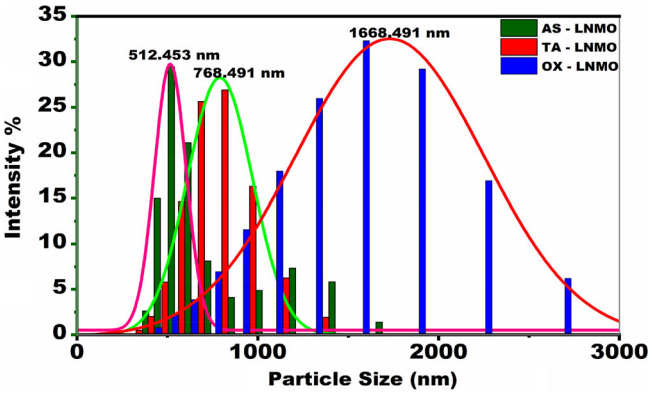

FIGURE 4 Representation of the Particle size distribution of Li $[Li_{0.2}Ni_{0.3}Mn_{0.7}]O_2$ prepared using different complexing agents

However, in the case of OX-LNMO a nano sheet was obtained with its own architecture. The finite crystal structure of samples AS-LNMO and TA-LNMO had numerous faces (surfaces) implied that a porous framework with a large surface area allows for a shorter lithium-ion diffusion length and hence results in enhanced electrochemical kinetics. Controlling the microstructure of particles or generating macroscale 3D structures on the other hand is a viable technique to improve electrochemical properties Figure S1. Two sets of lattice fringes were seen which indicated that two phases were coexisting. The regions denoted by squares were subjected to a fast Fourier transform (FFT). As observed in Figure S4 a pair of crystalline patterns of AS-LNMO had d-spacing of 0.472 nm and 0.144 nm corresponding to the (003) and (018) planes of the layered phase (R-3 m). The other phase had d-spacing of 0.208 nm corresponding to the cubic phase of the layered phase (R-3 m) (Fm-3 m). Figure S4 the FFT-filtered HRTEM nano graphs supplemented for sample TA-LNMO demonstrates that the lattice patterns of the Al matrix had d-spacing of 0.447 and 0.237 nm

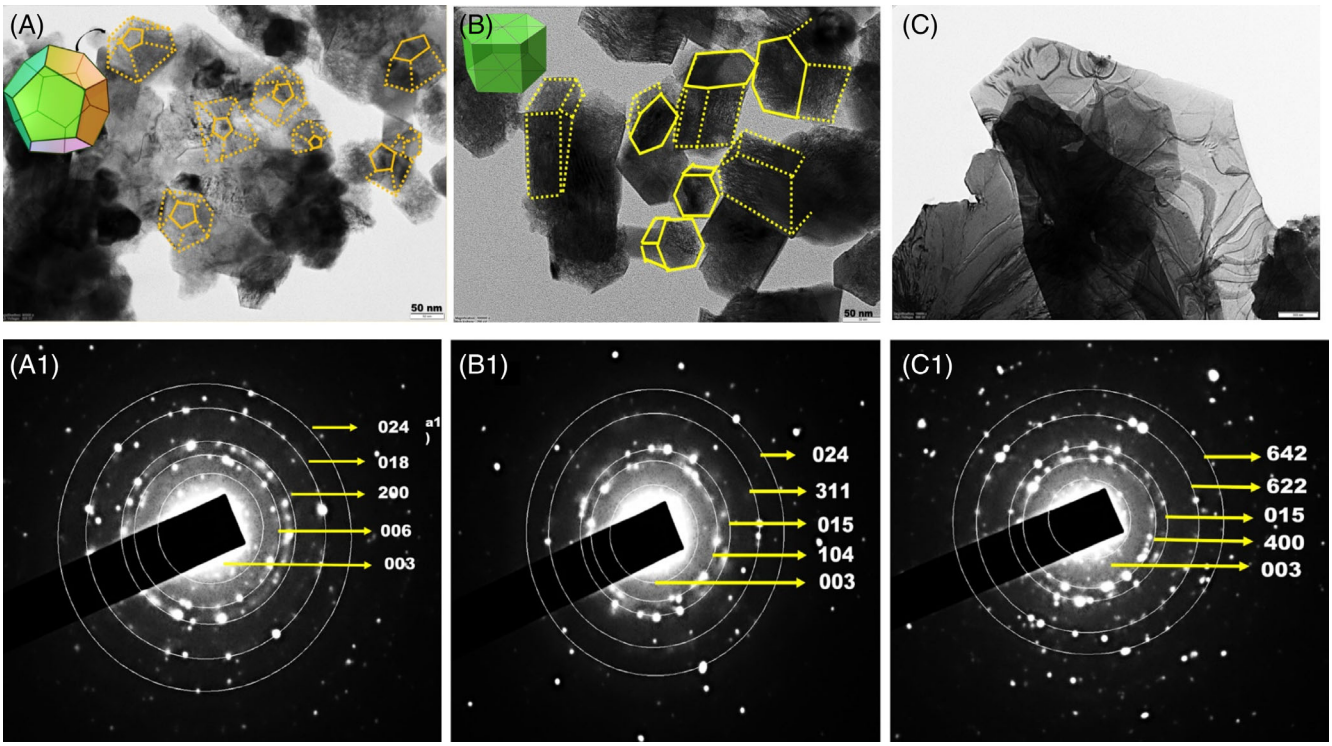

FIGURE 5 Representation of HR-TEM images of Li [Li $_{0.2}$ Ni $_{0.3}$ Mn $_{0.7}$] O_2 along with corresponding SAED pattern. (A, A1) AS-LNMO, (B, B1) TA - LNMO, (C, C1) OX-LNMO

corresponding to (003) and (006) planes of layer phase (R-3 m). The peripheral region had d-spacing of 0.24 nm corresponding to (111) plane of the cubic phase (Fm-3 m). Figure S4 the fringes in the sample OX-LNMO had d-spacing of 0.297 and 0.204 nm corresponding to the (220) and (400) planes of the spinel phase of Fd-3 m and 0.245 nm corresponding to the (101) plane of the layered phase of (R-3 m). According to the HRTEM data, the acquired particles were expected to be made up of two or three domains with distinct lattice fringes that corresponded to the layer, cubic, and spinel phases. AS-LNMO had the widest interlayer gap (0.472 nm) compared to TA-LNMO (0.447 nm) and OX-LNMO (0.297 nm). Lithium-ion intercalation benefits from large d-spacing since it ensures a low-energy barrier for lithium diffusion and results in a significant increase in specific capacity.[20,30-32]

3.2 | Electrochemical studies

3.2.1 | Galvanostatic charge/discharge (GCD) analysis

Charge/discharge curves of Li $[Li_{0.2}Ni_{0.3}Mn_{0.7}]$ O_2 samples synthesized via sol–gel method at different cycles are revealed in Figure 6A-C. The charge/discharge profiles were compatible with the electrochemical behavior of Li_2MnO_3-$LiN_{x-1}Mn_{1-x}O_2$ type lithium-rich manganese-based oxides (LMRO).

Their initial discharges were 180.86 $mhAg^{-1}$, 155.55 $mhAg^{-1}$, 143.04 $mhAg^{-1}$ which corresponded to AS-LNMO, TA-LNMO and OX-LNMO respectively. The multiphase samples exhibited a distinct phenomenon of increasing capacity with increasing cycle number during the initial cycles. Discharge capacities of the multiphase samples increased dramatically from their initial value of 180.86 $mhAg^{-1}$ (AS-LNMO) to 240.32 $mhAg^{-1}$ at 10th cycle. Further, it increased gradually to 260.43 $mhAg^{-1}$ at 50th cycle and reached to a.

stable capacity of 308.02 $mhAg^{-1}$. The same happened in the case of other two samples. According to these results, using different complexing agents had a major influence on the electrochemical performance of the prepared LNMO samples. The specific capacity of all the three samples was increased when the number of cycles increased. At the 100th cycle the discharge capacity of AS-LNMO - 308.02 $mhAg^{-1}$, TA-LNMO - 293.59 $mhAg^{-1}$, and OX-LNMO - 236.11 $mhAg^{-1}$ and their capacity retentions after 200 cycles were 95.2%, 99.3%, and 72.2% respectively. As per the previous report, LMRO cathode materials exhibited significant discharge

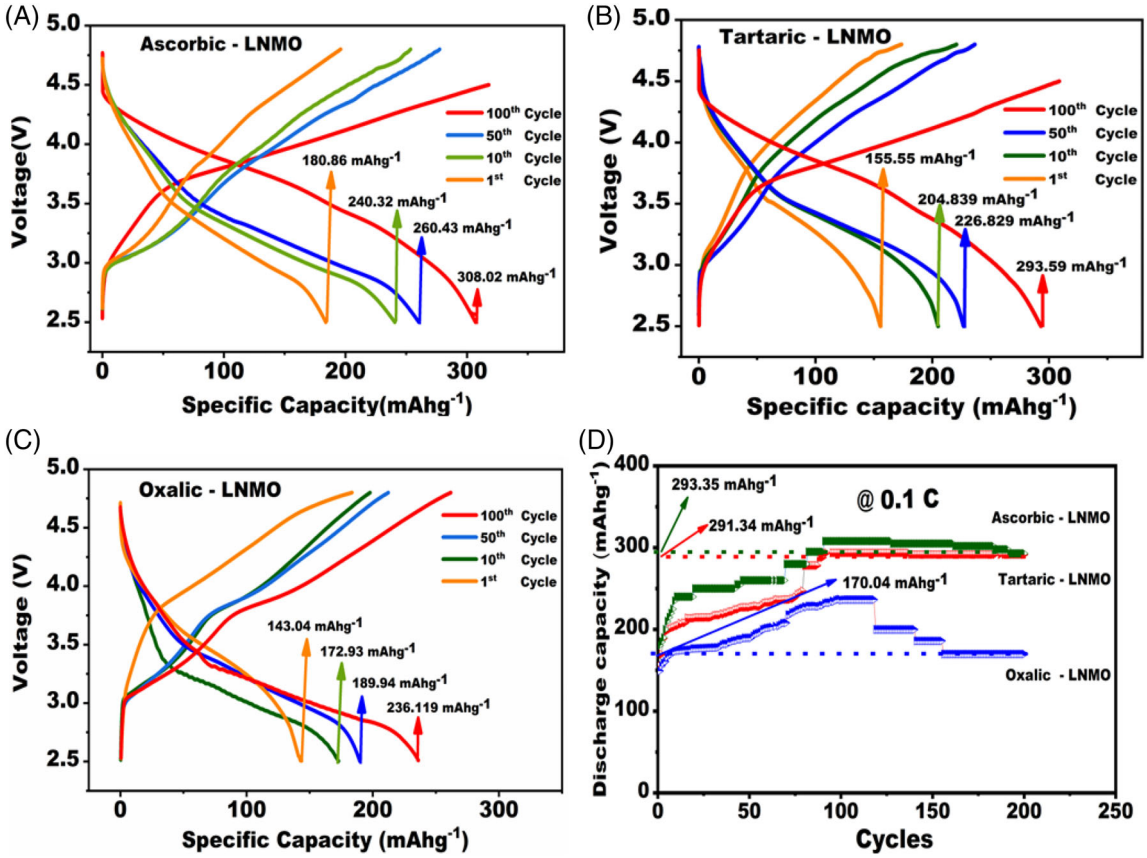

FIGURE 6 The charge/discharge profiles of Li $[Li_{0.2}\ Ni_{0.3}\ Mn_{0.7}]\ O_2$ prepared using different complexing agents at 0.1 c (A) AS-LNMO, (B) TA - LNMO, (C) OX-LNMO, (D) Cyclic performance of Li $[Li_{0.2}\ Ni_{0.3}\ Mn_{0.7}]\ O_2$ at 0.1 C

capacities ranging from 200 to >300 mhAg^{-1} at low to moderate C-rates.[18,23,33,34] Figure 6D each cathode complexed with three different complexing agents showed long cycling stability. The results show that after 200 cycles, TA-LNMO had the maximum capacity and cycling stability when compared to the other two samples. Whereas, the OX-LNMO had a worse cycling performance. This could be attributed to the thin nano sheet structure of OX-LNMO which is prone to damage after continuous cycling while AS-LNMO can start fading significantly from its original capacity value.

Rate capability $Li[Li_{0.2}Ni_{0.3}Mn_{0.7}]\ O_2$ with various complexing agents is depicted in Figure 7A. The specific discharge capacity of each electrode steadily declined with increasing current rate from 0.1C to 1C after the first activation of Li_2MnO_3 in the first cycle. In comparison to the other two TA-LNMO (197.48 mAhg^{-1}) and OX-LNMO (122.42 mAhg^{-1}), AS-LNMO appeared to charge and discharge at a maximum level of 228.22 mAhg^{-1} at 1C due to its highest carbon content which boosted up the conductivity.

Figure 7B represents the energy density of all the three samples. AS-LNMO with good conductivity due to its high carbon content and delivered a specific energy density of 962 WhKg^{-1} and TA-LNMO delivers 940 WhKg^{-1}. OX-LNMO with layered/spinel-like mixed state is associated with a large voltage drop which reduced the overall energy density of the material and resulted 690 WhKg^{-1}. Table 2 represents the quantitative elemental percentages of all the samples.

3.2.2 | Cyclic voltammetry analysis

Figure 7C shows the CV curves of LNMO samples complexed with different complexing agents. The overall electrochemical Ni^{2+}/Ni^{4+} couple was related with the cathodic oxidation peak at 4.6 V (AS-LNMO) and 4.4 V (TA-LNMO), while the spinel to rock-salt transformation was represented by the reduction peak at 2.8 V. The simultaneous lithium extraction and oxygen activation may be seen in the oxidation peak between 4.5 V and 4.8 V. Around 3.2 V, AS-LNMO and TA-LNMO showed smaller peaks corresponding to the spinel $Mn^{4+/}Mn^{3+}$. Nevertheless, the peak for AS-LNMO appeared to be less significant which caused capacity fading in later cycling.

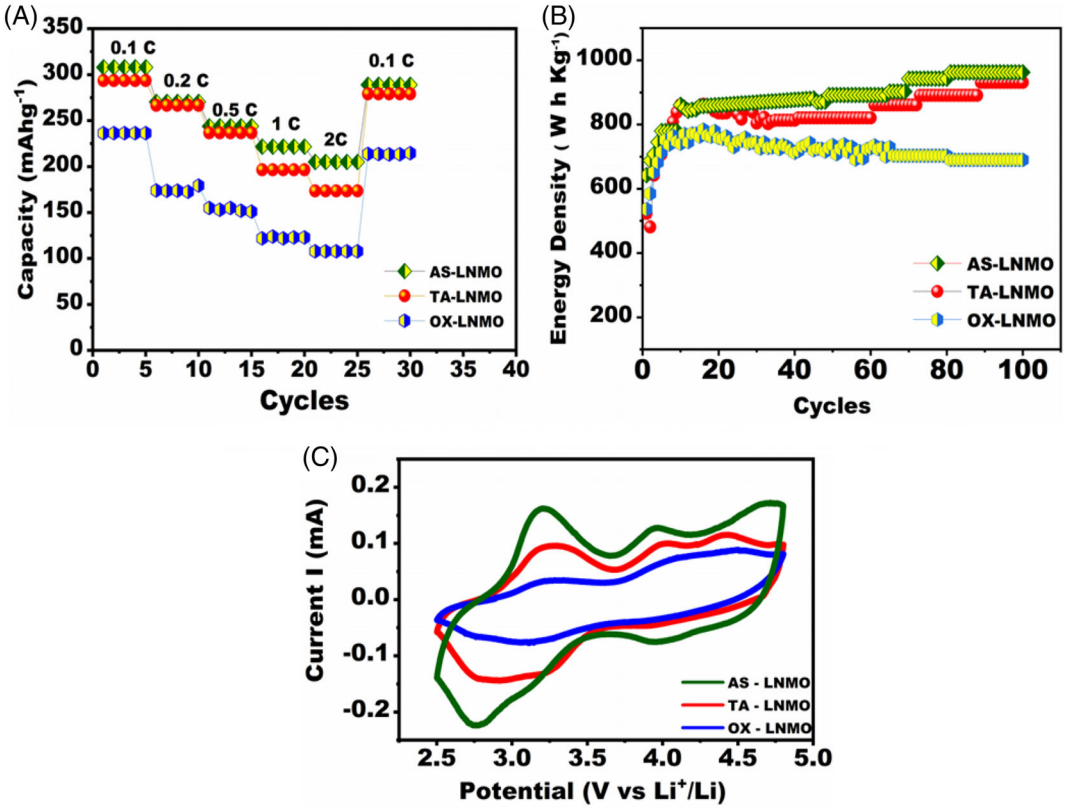

FIGURE 7 Representation of (A) Different C-rate (B) Energy density (C) CV curves of Li $[Li_{0.2}\ Ni_{0.3}\ Mn_{0.7}]\ O_2$ prepared using different complexing agents

TABLE 2 Quantitative values of elements present in Li $[Li_{0.2}Mn_{0.7}Ni_{0.3}]\ O_2$ prepared with different complexing agents

Samples	Elements	Wt%	At%
AS-LNMO	C	58.256	46.127
	O	30.623	42.168
	Mn	7.884	7.023
	Ni	3.360	4.682
		100.000	100.000
TA-LNMO	C	42.520	37.620
	O	45.931	50.251
	Mn	7.725	8.500
	Ni	3.824	3.629
		100.000	100.000
OX-LNMO	C	18.982	20.652
	O	72.021	68.603
	Mn	6.397	7.512
	Ni	2.600	3.233
		100.000	100.000

Leaching out of Li_xNi_{1-x} might have caused small oxidation peaks at 4 V corresponding to Mn^{4+}/Mn^{3+}.[31]

3.2.3 | Electrochemical impedance spectroscopy analysis

The AC impedance of the produced cathode materials was measured and the findings are presented in Figure 8A-C. Z View fitting software was used to create the equivalent circuit which is shown in Figure 8C. The AC impedance curve was divided into two parts: a semi-circle in the high frequency zone and a diagonal line in the low frequency region. The semi-circle corresponded to the charge transfer impedance (R_{ct}) of the material/electrolyte interface which includes the impedance of Li^+ in the electrolyte, separator and other inactive materials (R_s). Warburg impedance of lithium transport within the electrode and electrolyte was represented by the diagonal line. Figure 8A-C displayed the Nyquist plot described the impedance graphs of before cycling and after 100 cycles. From the results, it is evident that AS-LNMO has good conductivity and is reconfirmed in rate capability details which occurs due to the high content of carbon when compared to the other two samples.

The resistance values seemed to be decreasing after 100 cycles which ensured the increase of conductivity due to the unusual behavior exhibited by the samples in their cycling that is, the charging and discharging

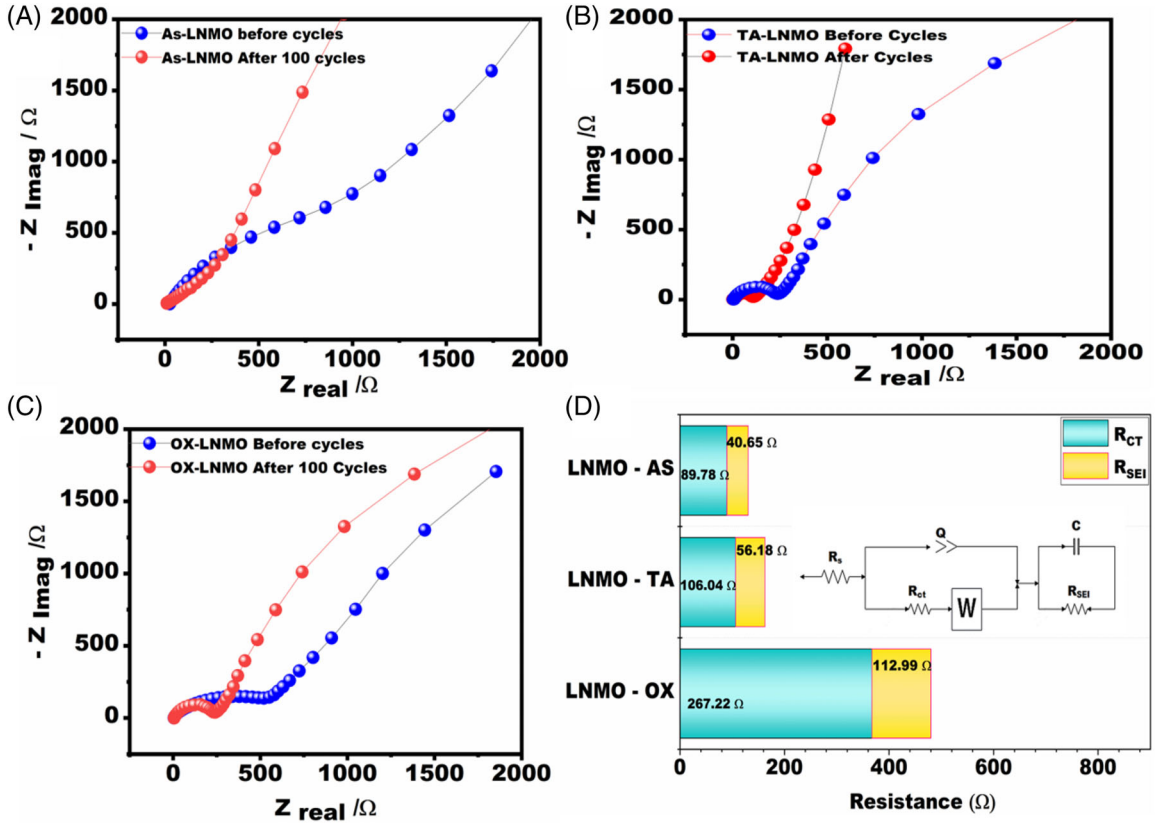

FIGURE 8 Nyquist plots of EIS spectra for of Li $[Li_{0.2}Ni_{0.3}Mn_{0.7}]O_2$ prepared using different complexing agents at 0.1 c (A) AS-LNMO, (B) TA - LNMO, (C) OX-LNMO (D) Resistance values after 100 cycles

capacity increased with number of cycles. In the discussion regarding R_{ct} and R_{SEI} values Figure 8D for all the three samples, AS-LNMO sample exhibited low R_{ct} value of 89.78 Ω followed by TA-LNMO of 106.04 Ω and OX-LNMO had the highest R_{ct} value of 267.22 Ω. This impedes the conductivity of the electrode very badly after 100 cycles. The low particle size, irregular porosity, and polyhedral faces leading to the enhanced surface area increased the conductivity of AS-LNMO and TA-LNMO cathode materials. The development of SEI surface has a massive effect on electrode material performance. On one hand, sections of the lithium ions are spent during the development of the SEI layer which increased the irreversible capacity of batteries while lowering the electrode material's charge and discharge efficiency. The SEI, on the other hand, was insoluble in organic solvents but can be stable in organic electrolyte solutions. Furthermore, solvent molecules were unable to travel through it thereby successfully preventing ion co-embedding and avoiding electrode material degradation. This considerably enhanced the battery's cycle performance and service life. In the AS-LNMO and TA-LNMO samples, the SEI film adds to structure and cycle stability. However, in OX-LNMO sample the extra passivation layer has caused capacity fading by raising the material's impedance. Another possible explanation could be, OX-LNMO had a thin nano sheet structure (analysed by HR-TEM) which could be broken by an aggressive reaction between the cathode and the electrode at a higher potential 4.8 V as a result of the creation of SEI layer in the electrode/electrolyte interface.

4 | CONCLUSION

Structure, morphology, particle size and electrochemical performance of Li $[Li_{0.2}Ni_{0.3}Mn_{0.7}]O_2$ were examined when different complexing agents were used for the synthesis procedure. All the samples had multi-phases with high crystallinity. The AS-LNMO sample was revealed to be the most effective in terms of achieving high capacity. The smaller the particle size, the greater number of Li_2MnO_3 was activated which resulted in the maximum capacity at various C-rates. The sample TA-LNMO was ranked second in particle size and had the highest capacity and best cycle stability. The sample OX-LNMO which had comparatively bigger particle size lost its ability to demonstrate itself to be a potential material due to

capacity fading. The samples AS-LNMO and TA-LNMO are restructured in the process of charging /discharging and materials ensure robust ordered hexagonal structure with good long cycling stability.

AUTHOR CONTRIBUTIONS

Prettencia L: Conceptualization, methodology, Investigation, writing-original draft preparation, analysis, visualization. Soundarrajan E: Data curation, investigation, formal analysis, software. Roselin Ranjitha M: Validation, writing – review &editing, formal analysis. Kalaivani RA: Investigation, supervision, resources. Raghu S: Methodology, Investigation, conceptualization, supervision, project administration, validation.

ACKNOWLEDGMENTS

We are grateful for the experimental facilities offered by the Centre for Alternative Energy and Fuels. We acknowledge the characterization services provided by SRM University. This research was supported by Vels Research Fellowship funding. And we are grateful for the valuable contribution of each author.

CONFLICT OF INTEREST

There are no conflicts to declare.

REFERENCE

1. Pan H, Zhang S, Chen J, et al. Li- and Mn-rich layered oxide cathode materials for lithium-ion batteries: a review from fundamentals to research progress and applications. *Mol Syst Des Eng*. 2018;3(5):748-803.
2. Li Y, Li Z, Chen C, et al. Recent progress in Li and Mn rich layered oxide cathodes for Li-ion batteries. *J Energy Chem*. 2021; 61:368-385.
3. Kim IT, Knight JC, Celio H, Manthiram A. Enhanced electrochemical performances of Li-rich layered oxides by surface modification with reduced graphene oxide/AlPO4 hybrid coating. *J Mater Chem A*. 2014;2(23):8696-8704.
4. Li S, Fu X, Liang Y, et al. Enhanced structural stability of boron-doped layered@spinel@carbon Heterostructured lithium-rich manganese-based cathode materials. *ACS Sustain Chem Eng*. 2020;8(25):9311-9324.
5. di Zhang Y, Li Y, Niu XQ, et al. A peanut-like hierarchical micro/nano-Li1.2Mn0.54Ni0.18Co0.08O2 cathode material for lithium-ion batteries with enhanced electrochemical performance. *J Mater Chem A*. 2015;3(27):14291-14297.
6. Wang D, Belharouak I, Ortega LH, et al. Synthesis of high capacity cathodes for lithium-ion batteries by morphology-tailored hydroxide co-precipitation. *J Power Sources*. 2015;274: 451-457.
7. Zhuravlev VD, Pachuev AV, Nefedova KV, Ermakova LV. Solution-combustion synthesis of LiNi1/3Co1/3Mn1/3O2 as a cathode material for lithium-ion batteries. *Int J Self-Propagating High-Temperature Synth*. 2018;27(3):154-161.
8. Zhang L, Wu B, Li N, Mu D, Zhang C, Wu F. Rod-like hierarchical nano/micro Li1.2Ni0.2Mn 0.6O2 as high performance cathode materials for lithium-ion batteries. *J Power Sources*. 2013;240:644-652.
9. Widiyandari H, Sukmawati AN, Sutanto H, Yudha C, Purwanto A. Synthesis of LiNi0.8Mn0.1Co0.1O2 cathode material by hydrothermal method for high energy density lithium ion battery. *J Phys Conf Ser*. 2019;1153(1):012074.
10. Zhou D, Li J, Chen C, Lin F, Wu H, Guo J. A hydrothermal synthesis of Ru-doped LiMn1.5Ni0.5O4cathode materials for enhanced electrochemical performance. *RSC Adv*. 2021;11(21): 12549-12558.
11. Zhang Y, Xie H, Jin H, et al. Enhancing the electrochemical properties of Ti-doped LiMn2O4Spinel cathode materials using a one-step hydrothermal method. *ACS Omega*. 2021;6(33): 21304-21315.
12. Zhu Z, Zhu L. Synthesis of layered cathode material 0.5Li2MnO 3·0.5LiMn1/3Ni1/3Co1/3O 2 by an improved co-precipitation method for lithium-ion battery. *J Power Sources*. 2014;256:178-182.
13. Krumdick, G.K., Shin, Y.H., and Feridun, O.K. (2013) Process Development and Scale-Up of Advanced Cathode Materials. *Argonne National Laboratory*. 23.
14. Daniel C, Mohanty D, Li J, Wood DL. (2014) cathode materials review. *AIP Conf Proc*. 2015;1597:26-43.
15. Sun Y, Shiosaki Y, Xia Y, Noguchi H. The preparation and electrochemical performance of solid solutions LiCoO2-Li2MnO3 as cathode materials for lithium ion batteries. *J Power Sources*. 2006;159(2):1353-1359.
16. Uddin MJ, Alaboina PK, Cho SJ. Nanostructured cathode materials synthesis for lithium-ion batteries. *Mater Today Energy*. 2017;5:138-157.
17. Ates MN, Mukerjee S, Abraham KM. A high rate Li-rich layered MNC cathode material for lithium-ion batteries. *RSC Adv*. 2015;5(35):27375-27386.
18. Dong P, Xia SB, Zhang YJ, Zhang YN, Qiu ZP, Yao Y. Influence of complexing agents on the structure and electrochemical properties of LiNi0.80Co0.15Al0.05O2 cathode synthesized by sol-gel method: a comparative study. *Int. J. Electrochem. Sci.* 2017;12(1):561-575.
19. Kim Y, Kim D. Synthesis of high-density nickel cobalt aluminum hydroxide by continuous coprecipitation method. *ACS Appl Mater Interfaces*. 2012;4(2):586-589.
20. Zhao C, Shen Q. Organic acid assisted solid-state synthesis of Li1.2Ni0.16Co0.08Mn0.56O2 nanoparticles as lithium ion battery cathodes. *Curr Appl Phys*. 2014;14(12):1849-1853.
21. Hua W, Wang S, Knapp M, et al. Structural insights into the formation and voltage degradation of lithium- and manganese-rich layered oxides. *Nat Commun*. 2019;10(1):1-11.
22. Guan C, Huang H. Complexing agents on carbon content and lithium storage capacity of LiFePO4/C cathode synthesized via sol-gel approach. *Adv Mater Sci Eng*. 2016;2016:7.
23. Wang J, Xia Y, Yao X, Zhang M, Zhang Y, Liu Z. Synthesis and electrochemical feature of a multiple-phases Li-rich nickel manganese oxides cathode material. *Int J Electrochem Sci*. 2011;6(12):6670-6681.
24. Reed J, Ceder G, Van Der Ven A. Layered-to-spinel phase transition in LixMnO2. *Electrochem Solid St*. 2001;4(6):2-6.
25. Sigel F, Schwarz B, Kleiner K, et al. Thermally induced structural reordering in Li- and Mn-rich layered oxide Li ion cathode materials. *Chem Mater*. 2020;32(3):1210-1223.

26. Jarvis KA, Wang CC, Knight JC, Rabenberg L, Manthiram A, Ferreira PJ. Formation and effect of orientation domains in layered oxide cathodes of lithium-ion batteries. *Acta Mater*. 2016; 108:264-270.
27. Capone I, Hurlbutt K, Naylor AJ, Xiao AW, Pasta M. Effect of the particle-size distribution on the electrochemical performance of a red phosphorus-carbon composite anode for sodium-ion batteries. *Energy Fuels*. 2019;33(5):4651-4658.
28. Bläubaum L, Röder F, Nowak C, Chan HS, Kwade A, Krewer U. Impact of particle size distribution on performance of lithium-ion batteries. *ChemElectroChem*. 2020;7(23):4755-4766.
29. Massé RC, Liu C, Li Y, Mai L, Cao G. Energy storage through intercalation reactions: electrodes for rechargeable batteries. *Natl Sci Rev*. 2017;4(1):26-53.
30. Dou S, Li P, Li H. Hollow microspherical Li [Li0.24Ni0.38Mn0.38]O2 as cathode material for lithium-ion batteries with excellent electrochemical performance. *Int. J. Electrochem. Sci.* 2018;13(10):9654-9668.
31. Science M, Cao G, Cheng-Yan X. Phase transition induced synthesis of layered/spinel heterostructure with enhanced electrochemical properties. *Adv Energy Mater*. 2017;27(7):1604349.
32. Lee W, Muhammad S, Sergey C, et al. Advances in the cathode materials for lithium rechargeable batteries. *Angew Chemie - Int ed*. 2020;59(7):2578-2605.
33. Akhilash M, Salini PS, John B, Mercy TD. A journey through layered cathode materials for lithium ion cells – from lithium cobalt oxide to lithium-rich transition metal oxides. *J Alloys Compd*. 2021;869:159239.
34. Das H, Urban A, Huang W, Ceder G. First-principles simulation of the (Li-Ni-vacancy)O phase diagram and its relevance for the surface phases in Ni-rich Li-ion cathode materials. *Chem Mater*. 2017;29(18):7840-7851.

SUPPORTING INFORMATION

Additional supporting information can be found online in the Supporting Information section at the end of this article.

How to cite this article: Prettencia LJ, Soundarrajan E, Roselin Ranjitha M, Kalaivani R, Raghu S. Sol-gel route synthesis of high energy density Li $[Li_{0.2}Ni_{0.3}Mn0_{.7}]$ O_2 cathode with controlled structure, morphology and enhanced electrochemical performance. *Energy Storage*. 2022; e427. doi:10.1002/est2.427